Precision Clinical Medicine, 2024, **7**: pbae011

DOI: 10.1093/pcmedi/pbae011

Research Article

Depletion of squalene epoxidase in synergy with glutathione peroxidase 4 inhibitor RSL3 overcomes oxidative stress resistance in lung squamous cell carcinoma

Guo Li,[1,2,†] Lu Chen,[2,†] Hua Bai,[1] Li Zhang,[2,3,4,5,*] Jie Wang,[1,*] Weimin Li[2,3,4,5,6,*]

[1]CAMS Key Laboratory of Translational Research on Lung Cancer, State Key Laboratory of Molecular Oncology, Department of Medical Oncology, National Cancer Center/National Clinical Research Center for Cancer/Cancer Hospital, Chinese Academy of Medical Sciences Peking Union Medical College, Beijing 100021, China
[2]Department of Pulmonary and Critical Care Medicine, West China Hospital, Sichuan University, Chengdu 610041, China
[3]Institute of Respiratory Health, Frontiers Science Center for Disease-related Molecular Network, West China Hospital, Sichuan University, Chengdu 610041, China
[4]Precision Medicine Center, Precision Medicine Key Laboratory of Sichuan Province, West China Hospital, Sichuan University, Chengdu 610041, China
[5]State Key Laboratory of Respiratory Health and Multimorbidity, West China Hospital, Chengdu 610041, China
[6]The Research Units of West China, Chinese Academy of Medical Sciences, West China Hospital, Chengdu 610041, China
*Corresponding authors: Li Zhang, zhangli2809@wchscu.cn; Jie Wang, zlhuxi@163.com; Weimin Li, Weimin003@163.com
†Guo Li and Lu Chen contributed equally to this work.

Abstract

Background: Lung squamous cell carcinoma (LUSC) lacks effective targeted therapies and has a poor prognosis. Disruption of squalene epoxidase (SQLE) has been implicated in metabolic disorders and cancer. However, the role of SQLE as a monooxygenase involved in oxidative stress remains unclear.

Methods: We analyzed the expression and prognosis of lung adenocarcinoma (LUAD) and LUSC samples from GEO and TCGA databases. The proliferative activity of the tumors after intervention of SQLE was verified by cell and animal experiments. JC-1 assay, flow cytometry, and Western blot were used to show changes in apoptosis after intervention of SQLE. Flow cytometry and fluorescence assay of ROS levels were used to indicate oxidative stress status.

Results: We investigated the unique role of SQLE expression in the diagnosis and prognosis prediction of LUSC. Knockdown of SQLE or treatment with the SQLE inhibitor terbinafine can suppress the proliferation of LUSC cells by inducing apoptosis and reactive oxygen species accumulation. However, depletion of SQLE also results in the impairment of lipid peroxidation and ferroptosis resistance such as upregulation of glutathione peroxidase 4. Therefore, prevention of SQLE in synergy with glutathione peroxidase 4 inhibitor RSL3 effectively mitigates the proliferation and growth of LUSC.

Conclusion: Our study indicates that the low expression of SQLE employs adaptive survival through regulating the balance of apoptosis and ferroptosis resistance. In future, the combinational therapy of targeting SQLE and ferroptosis could be a promising approach in treating LUSC.

Keywords: lung squamous cell carcinoma; squalene epoxidase; terbinafine; ROS; ferroptosis

Introduction

Lung squamous cell carcinoma (LUSC) is a subtype of non-small cell lung cancer (NSCLC) that represents 20%–30% of all NSCLC cases. LUSC exhibits indolent progression in the early stages, and substantial advancements in targeted therapeutic strategies for LUSC are lacking. LUSC is characterized by multiple driver mutations, including *nuclear receptor binding SET domain protein 3 (NSD3)* mutations, *fibroblast growth factor receptor 1 (FGFR1)* amplification, *phosphatidylinositol-3 kinase (PI3K)* pathway mutations and G1/S checkpoint mutations [1–3]. The prevalence of potentially druggable target variants is as high as 60%, but failure is inevitable in almost all clinical trials. Recently, therapies targeting metabolic vulnerabilities, such as those targeting gluconeogenesis or lipid synthesis, have been proposed for LUSC [4, 5]. Therefore, discovering new metabolic targets is critical to diagnosing and treating LUSC.

The synthesis of cholesterol has been demonstrated in tumorigenesis, metastasis and acquiring drug resistance. Lipid-lowering statins can effectively alleviate chemoresistance in patients with recurrent small cell lung cancer [6]. Xu *et al.* previously showed that squalene epoxidase (SQLE), the enzyme with the second highest rate-limiting contribution to cholesterol synthesis, maintains cholesterol-dependent lipid raft structures and promotes the activation of the Src/PI3K/AKT signalling pathway, which is causally connected with the development of pancreatic cancer [7]. Moreover, SQLE could promote the development of hepatocellular carcinoma (HCC) through epigenetic reprogramming induced by reactive oxygen species (ROS) accumulation [8]. In contrast, SQLE has also been reported to exert an inhibitory effect on tumor metastasis, implying that knockdown of SQLE can promote disseminated metastasis of colorectal cancer (CRC) by inducing epithelial-mesenchymal transition (EMT) [9].

Received 12 March 2024; accepted 29 April 2024. published 8 May 2024

Therefore, whether SQLE promotes cancer progression remains unclear.

The involvement of ROS in cancer is multifaceted and encompasses the regulation of metabolic and signalling pathways [10], such as the PI3K, AKT and protein kinase C (PKC) pathways, as well as the activation of various transcription factors, including nuclear factor erythroid 2-related factor 2 (NFE2L2, also known as NRF2), HIF1α, NF-κB and p53 [11–13]. Therefore, the activation of ROS signalling can contribute to multiple aspects of cancer progression. Ferroptosis is an Fe^{2+}-dependent lipid peroxidation that is also reliant on ROS. Excessive lipid peroxidation may initiate cell death by injuring the cell membrane [14, 15]. However, there are also reports suggesting that the reducing substances such as squalene attending this process can protect cells from ferroptosis [16].

The exact mechanism by which SQLE controls oxidative stress remains unknown despite reports of a link between SQLE expression and the production of ROS. Furthermore, whether SQLE influences oxidative stress resistance or not is also unclear. In this study, we found that prevention of SQLE suppressed the development LUSC *in vivo* and *in vitro*, predominantly though endogenous apoptosis and overabundance of ROS. However, SQLE deletion might activate glutathione peroxidase 4 (GPX4), which in turn promotes lipid peroxidation resistance to counteract excessive oxidative stress. Therefore, targeting SQLE in combination with the GPX4 inhibitor RSL3 could be a therapeutic strategy for LUSC.

Materials and method

Cell lines and reagents

The human lung adenocarcinoma (LUAD) and LUSC cell lines including HCC827, H1975, PC9, H1299, A549, SK-MES-1, Calu-1 and H226 used in the experiments were purchased from the American Type Culture Collection (ATCC) and approved by Short Tandem Repeat (STR) prior to the experiments. The cells were grown in RPMI-1640 medium (GIBCO) supplemented with 10% Fetal Bovine Serum (FBS) (GIBCO) at 37°C in a humidification chamber containing 5% CO_2.

Cell viability, migration and invasion

Cell viability: different groups of cells were plated in 96-well plates at 2000–3000 cells per well at different time points of cell culture or after drug treatment, and cell counting kit-8 (CCK-8) solution was added to the medium (1 : 10) and incubated at 37°C for 2 h. Absorbance was measured at 450 nm with a microtiter reader (BioTek, Winooski, VT). CCK-8 was purchased from APExBIO (K1018).

Cell invasion: different groups of SQLE inhibitor-treated cells were cultured into the logarithmic proliferative phase, and then the cells were digested and aliquots were transferred into FALCON transwell chambers (24-well culture plates, Corning). The invasion assay required the addition of matrix gel to the chambers 4 h in advance. The upper layer was serum-free medium and the lower layer contained a high concentration of serum (15% FBS). Colonies were quantified using ImageJ software after fixation and staining with 1% crystal violet.

Cell migration: cells were spread into six-well plates at 3×10^5 counts, and after fusing into a monolayer, parallel lines were drawn on the bottom of the six-well plate with a marker pen. Consistent scratches on the different groups of cells were created along with parallel lines using a yellow pipette tip (200 μl) and washed twice with PBS. Then the cells were incubated using 1640 medium with a low serum concentration (2% FBS). The cells were observed and photographed at 0 and 24 h.

ROS staining and detection

Cells were first washed with PBS followed by 2.5 μM CellROX™ Deep Red (Invitrogen™ Catalog No.C10422) in working solution. After incubation for 30 min at 37°C the stained cells were then washed again with PBS and ROS were detected by flow cytometry.

Western blot

Total protein was extracted using a bicinchoninic acid (BCA) assay kit by lysing cell precipitates with RIPA lysis buffer for 10–20 min on ice or at 4°C, followed by centrifugation at 12 000 × g for 15 min at 4°C. The protein lysate was diluted in 5X loading buffer and denatured by boiling at 100°C for 5–10 min. Protein samples (60 μg) were separated by sodium dodecyl sulfate-polyacrylamide gel electrophoresis (SDS-PAGE) and transferred to a polyvinylidene difluoride (PVDF) membrane by membrane transfer on ice at 250 mA. They were blocked with 5% nonfat milk for 1–2 h followed by incubation with primary antibodies overnight at 4°C in an orbital shaker. The membrane was incubated with goat anti-rabbit or anti-mouse IgG secondary antibody for 1–2 h at 4°C on an orbital shaker after primary antibody was washed off. Finally, the membrane was visualized with a chemiluminescence imager and exposed to the enhanced chemiluminescence (ECL) dye solution.

Primary antibodies used included: anti-SQLE (Proteintech, Cat# 12544–1-AP), anti-β-actin (BIOX, Cat# BX-009), anti-caspase 3 (CST, Cat# 9662S), anti-cleaved caspase 3 (CST, Cat# 9664T), anti-caspase 9 (Proteintech, Cat# 10380–1-AP), anti-GPX4 (CST, Cat# 52455S), anti-xCT (abcam, ab175186), anti-Bcl2 (CST, Cat# 15071T), and anti-BAX (CST, Cat# 5023T).

Immunohistochemical analysis

Tissue sections were baked at 60°C, paraffinized with xylene and hydrated with decreasing graded ethanol solutions (100, 95, 85 and 75%) and ddH_2O. For antigen repair, sections were immersed in citrate buffer (pH 6. 0), then tissue sections were treated with microwave, endogenous peroxidase was blocked with 3% hydrogen peroxide and serum was blocked. Primary antibody was incubated overnight. Primary antibodies used included: anti-SQLE (Proteintech, Cat# 12544–1-AP) and anti-Ki67 (CST, Cat# 12202T).

Lentiviral infection and RNA interference of gene expression

Small interfering RNA (siRNA) and short hairpin RNA (shRNA) targeting SQLE and transfection reagent were purchased from Hanheng Biotechnology (Shanghai, China). Human siRNA and shRNA target sequences were: SQLE#1: GGATAAAGAGACTGGAGAT; SQLE#2: GCAGAGCCCAATGCAAAGTTT; and SQLE-siRNA#3: GCACCACAGTTTAAAGCAAAT; and human gRNA1: GCAGCTGTGCTTTCCAGAGA.

Mitochondrial membrane potential (MMP) assay

SQLE-KO and control Calu-1 cells were seeded and cultured in black 96-well plates (Perkinelmer 6055300) in the incubator after 48 hours. Next, cells were washed with PBS and incubated with reagents from JC-1 kits (UelandyJ6004L) at 37 °C for 30 min. Then, the reagent was gently removed, and cells were washed with washing buffer of the kit. 100 μL/well of PBS was added and the fluorescence was measured at 585/590 nm (red fluorescence) and 510/527 nm (green fluorescence) using a high-content screening system of a confocal microscope (HCSSCM). Mitochondrial

membrane potential was estimated by measuring the fluorescence of free JC-1 monomers (green) and JC-1 aggregates in mitochondria (red) and the results were expressed as the ratio of the aggregates/monomers of JC-1 in the percentage of control. Mitochondrial depolarization was indicated by a decrease in the polymer/monomer fluorescence intensity ratio.

Targeted metabolomic analysis for squalene

Targeted metabolomic analysis was performed on the Nexera LC30A UHPLC system coupled with an AB Sciex triple quadrupole (QqQ) 6500 mass spectrometer (Framingham, MA, USA). Chromatographic separation was performed on a Waters BEH Amide column (2.1 × 100 mm, 1.7 μm, Waters, Milford, MA, USA) at 35°C. Squalene was detected by multiple reaction monitoring mode. Data were acquired using Analyst 1.7.2™ software and analyzed using Multiquant 3.0.2 software (AB Sciex, Framingham, MA, USA).

Animal experiments

The Animal Care and Use Committee approved all animals for use in the studies included in this project. The gender of the experimental animals had no direct effect on the results. All experimental animals were male mice. Mice used in the xenograft model were 6-week-old male DBA2J mice purchased from Gempharmatech (China, Jiangsu). KLN205 cells (3×10^6) were resuspended with 100 μl PBS and then injected into the subcutaneous tissue of the right thigh of the mice. After 6 days, tumor formation was seen subcutaneously and treated with terbinafine (TBF) and PBS (vehicle) by intraperitoneal injection at 80 mg/kg every other day (q2d). The size of the tumor mass was evaluated every 2 days, and was calculated using the formula: volume = 0.5 × length × width^2. The mice were euthanized at the end of the study.

Expression profiles and gene set enrichment analysis

The gene expression profiles of GSE43580 and GSE4573 were obtained from the Gene Expression Omnibus (GEO, http://www.ncbi.nlm.nih.gov/geo/). The human lung cancer data sets from The Cancer Genome Atlas (TCGA) (Firehose Legacy) were obtained from the cBioPortal for Cancer Genomics (http://cbioportal.org). In order to identify the pathways of interest for the differentially expressed genes between the high and low SQLE expression groups of lung cancer samples from the TCGA dataset, a gene set enrichment analysis (GSEA) was performed. The gene sets were retrieved from MSigDB (https://www.gsea-msigdb.org/gsea/msigdb), which can be found on the GSEA web site.

Statistical analysis

Except for animal experiments, all data are expressed as mean ± standard error of the mean (SEM) from at least three independent experiments. R (version 4.0.3) and GraphPad Prism (version 10.1.2) software were used for statistical analysis. Unpaired or paired two-tailed Student's t-tests were used for comparisons between groups. The Kaplan–Meier method was used for analysis of survival and the log-rank test was used to calculate the significance of the differences. The correlation between genes was measured by Pearson's correlation. $P < 0.05$ was regarded as a statistically significant difference.

Results

SQLE differential expression in NSCLC

To find out whether SQLE is the vulnerable point of cholesterol metabolism in lung cancer, we analyzed proteomic data of paired cancer and normal adjacent tissue (NAT) from 30 LUAD and 30 LUSC patients. We observed that steroid hormone biosynthesis was one of the most prominent pathways in patients with LUSC using the hallmark pathway of normalized gene-set enrichment score (NES) and GSEA (Fig. 1A). As steroid hormone biosynthesis and cholesterol biosynthesis share the same synthetic pathway, we investigated whether SQLE, the second step enzyme in cholesterol synthesis, might be a potential target for LUSC. Apparently, SQLE was considerably overexpressed in cancer (CA) compared with NAT in LUSC (Fig. 1B, supplementary Table S1, see online supplementary material), whereas LUAD-CA results lacked significant difference compared to LUSC-NAT (Fig. 1C, supplementary Table S1). Moreover, SQLE was highly expressed in LUSC-CA compared with LUAD-CA (Fig. 1D, supplementary Table S1). In addition, the expression level of SQLE among many tissue malignancies was found to be higher than that in the NATs (Fig. 1E). An integrated analysis of TCGA and Genotype-Tissue Expression (GTEx) databases was conducted to investigate the differential expression of SQLE between the cancer tissues and NATs of clinical NSCLC samples. SQLE was substantially overexpressed in LUSC but not in LUAD (Fig. 1F). Regarding clinical stage, SQLE expression in patients with stages I–II and stages III–IV of LUSC was significantly increased compared with that in normal controls. Additionally, SQLE expression was marginally higher in patients with stages III–IV than in patients with stages I–II (Fig. 1G). However, there was no discernible change in SQLE expression between the LUAD groups (Fig. 1H). Consequently, SQLE is predominantly highly expressed in LUSC.

High expression of SQLE can predict the diagnosis and prognosis of LUSC

To further validate the expression in clinical samples, we assembled 45 clinical samples of LUSC ($n = 30$) and LUAD ($n = 15$), which revealed that SQLE expression exhibited a moderate to strong intensity in the LUSC samples by immunohistochemical (IHC) staining (Fig. 2A), whereas it was more weakly positive in the samples of LUAD (Fig. 2B). The IHC scoring statistics also suggested that the percentage of SQLE-positive cells and SQLE expression intensity was higher in LUSC than in LUAD (Fig. 2C, supplementary Table S2, see online supplementary material).

The diagnostic value of SQLE in NSCLC was estimated by analyzing its expression. The results showed that SQLE expression had a high diagnostic performance in distinguishing tumorigenesis in LUSC [area under the curve (AUC) = 0.83, 95% confidence interval (CI) 0.79–0.87] compared to LUAD (AUC = 0.56, 95% CI 0.49–0.6) (Fig. 2D, E). To determine whether SQLE expression affects the prognosis for LUSC patients, we analyzed case data from the cbioportal database. Our findings indicate that LUSC patients in the SQLE-high group had worse overall survival (OS) compared to those in the SQLE-low group in the TCGA database. However, there was no significant difference in patients with LUAD (Fig. 2F). The disease-free survival (DFS) of LUSC with high SQLE expression compared to LUAD was indicative of a worse prognosis. This suggests that patients with high SQLE expression may relapse or experience metastasis at an early stage, according to Kaplan–Meier survival analysis of TCGA data (Fig. 2G). Multiple LUSC-associated cohorts in the GEO database, such as GSE4573 and GSE50081, reflect that patients with high levels of SQLE in LUSC have a worse

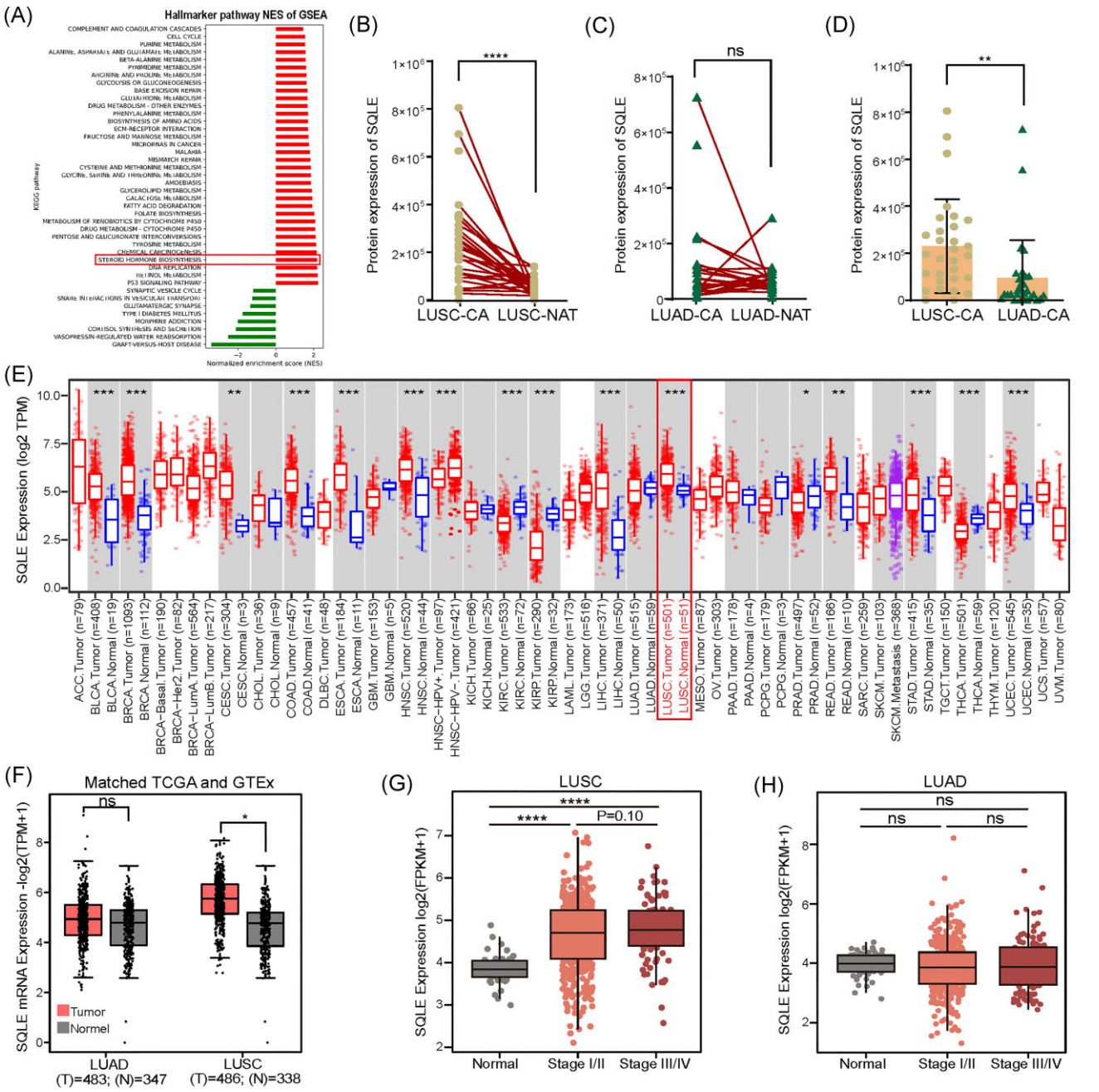

Figure 1. SQLE is highly expressed in LUSC compared to LUAD. (**A**) Bar plot showing the enrichment level of Kyoto Encyclopedia of Genes and Genomes (KEGG) pathways. Red bars represent significantly enriched KEGG pathways in LUSC samples, whereas green bars represent those significantly enriched in normal samples. (**B**–**D**) Proteomic data of SQLE in cancer and paired NAT from 30 LUAD and 30 LUSC patients. LUSC-NAT ($n = 30$) vs LUSC-CA ($n = 30$) (B); LUAD-NAT ($n = 30$) vs LUAD-CA ($n = 30$) (C); LUSC-CA ($n = 30$) vs LUAD-CA ($n = 30$) (D). Boxplots show the expression levels of SQLE mRNA in pan-cancer (**E**) and NSCLC (**F**) in the TCGA and GTEx databases. Boxplots show the differential expression of SQLE mRNA in different clinical stages of LUSC (**G**) and LUAD (**H**) patients in the TCGA database. *$P < 0.05$; **$P < 0.01$; ***$P < 0.001$; ****$P < 0.0001$; ns not significant.

prognosis (supplementary Fig. S1A, B, see online supplementary material). Therefore, there is a significant correlation between SQLE expression and the risk of LUSC, making it a potentially important target for LUSC development.

SQLE promotes the proliferation, migration and invasion of LUSC cell lines

To investigate the role of SQLE in tumor cell lines, we examined the expression of SQLE in a series of LUAD (HCC827, H1975, PC-9, A549, H1299) and LUSC (SK-MES-1, Calu-1, H226) cell lines as well as in the normal alveolar bronchial epithelial cell line BEAS-2B. The findings illustrated that SQLE expression was higher in LUSC compared to LUAD cell lines. (Fig. 3A). Additionally, the SK-MES-1 cell lines were used to construct SQLE knockdown (SQLE-KD) through the use of shRNA targeting SQLE (sh-SQLE) (Fig. 3B). Notably, we discovered that SQLE-KD could lessen cell proliferation and invasion (Fig. 3C, D). Stable transfected cell lines with SQLE overexpression (SQLE-OE) were constructed for Calu-1 and H226 (Fig. 3E, Supplementary Fig. S2A, B). In contrast, SQLE-OE

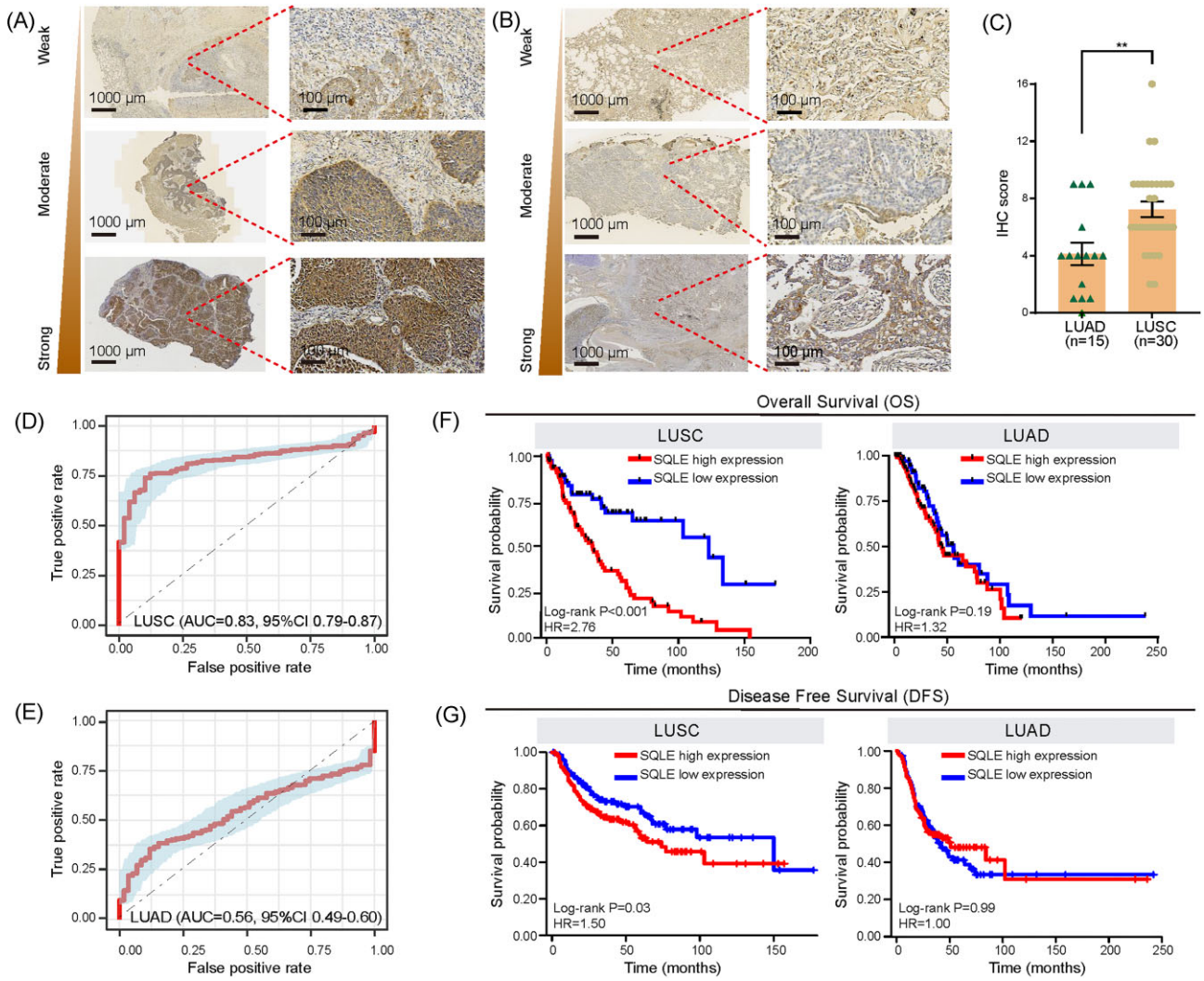

Figure 2. High expression of SQLE is closely correlated to poor prognosis in LUSC compared to LUAD. Representative image of IHC and statistical analysis of patients with LUAD ($n = 15$) (**A**) and LUSC ($n = 30$) (**B**). Statistical analysis of IHC score (**C**). Receiver operating curve of the SQLE gene in distinguishing normal from tumor patients in LUSC (**D**) and LUAD (**E**). Kaplan–Meier curves of OS (**F**) and DFS (**G**) in LUSC and LUAD samples with low and high SQLE expression in the TCGA database. ** $P < 0.01$

had the capacity to boost cell invasion of Calu-1 (Fig. 3F) as well as cell proliferation in Calu-1 and H226 cells (Fig. 3G). Furthermore, wound healing experiments showed that SQLE-KD could significantly hamper the migratory capacity after 24 h in comparison with that of the sh-scramble group in SK-MES-1 cells (Fig. 3H). On the other hand, SQLE-OE facilitated wound healing compared with that of the control in H226 cells (Fig. 3I). Consequently, we verified that suppression of SQLE significantly impaired proliferation, migration and invasion in LUSC cells.

Therapeutic effect of SQLE inhibitor TBF in vitro and in vivo

To further understand the therapeutic efficacy of SQLE inhibitors (SQLEi) in LUSC, two SQLEi, TBF and NB-598, were examined both *in vitro* and *in vivo*, as they have been previously reported to be used for pharmacological treatment of various malignancies [17, 18]. The following method was used to determine the half maximal inhibitory concentration (IC_{50}) of TBF and NB-598 in three LUSC cell lines, including H226, SK-MES-1 and Calu-1. TBF was given at progressively higher concentrations: 0, 5, 10, 20, 40, 60, 80, 100 and 120 μM. In a similar manner, NB-598 also was given in escalating doses from 0, 0.25, 0.5, 1, 2, 4, 6, 8, 10 to 12 μM. The approximate IC_{50} values for TBF and NB-598 in three cell lines were 50-60 μM and 6-8 μM, respectively (Fig. 4A, B). Thereafter, we implemented distinct gradients of concentration (30 and 60 μM for TBF, 3 and 6 μM for NB-598) for these two drugs, respectively. With the dose- and time-dependent conditions, the proliferative viability of the SQLEi-treated group was markedly repressed in comparison to the control group (with the addition of Dimethyl Sulfoxide (DMSO)) (Fig. 4C). Similarly, there was an appreciable suppression of invasion after treatment with TBF and NB-598 for 48 h in increasing doses, respectively (Fig. 4D, E, F and G). Surprisingly, it was also discovered that the protein expression of SQLE was not eliminated and was even elevated after the addition of SQLEi (Supplementary Fig. S2C). This phenomenon was also in line with a previous study (Fig. 5C) that showed that adding TBF and NB-598 for 24 h may enhance the generation of SQLE protein [19]. It could be hypothesized that SQLEi might stimulate SQLE expression by activating some unknown mechanisms that exceeded the pharmacological inhibitory effect.

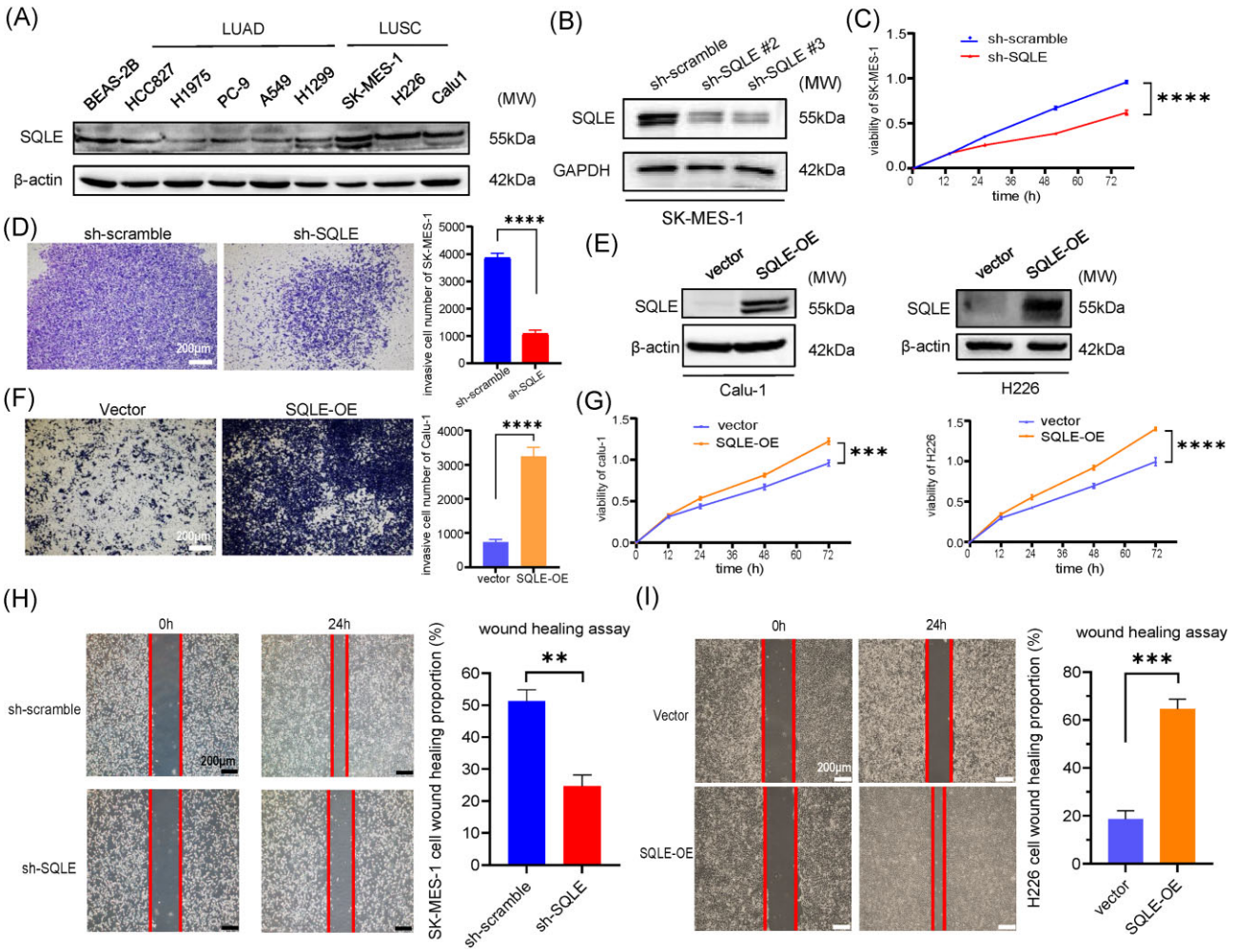

Figure 3. SQLE promotes LUSC proliferation, migration and invasion. (**A**) Western blotting analysis showing normal alveolar bronchial epithelial cell line BEAS-2B, LUAD cell lines such as HCC827, H1975, PC-9, A549 and H1299, and LUSC cell lines including SK-MES-1, Calu-1 and H226. (**B**) SQLE protein levels were examined in SK-MES-1 cells expressing scramble or SQLE shRNA via western blotting. (**C**) Growth curves of SK-MES-1 cells expressing sh-scramble or shRNA of SQLE by CCK-8 assay. (**D**) Crystal violet staining for cell invasion experiment and statistical plot of SK-MES-1 cells expressing sh-scramble or shRNA of SQLE via transwell chambers. Scale bar: 200 μm. (**E**) SQLE protein levels of H226 and Calu-1 cells expressing vector or SQLE overexpression were examined via western blott analysis. (**F**) Crystal violet staining for cell invasion experiment and statistical plot of Calu-1 cells expressing vector or SQLE overexpression via transwell chambers. Scale bar: 200 μm. (**G**) Growth curves of H226 and Calu-1 cells expressing vector or SQLE overexpression by CCK-8 assay. (**H**) Migration capacity of SK-MES-1 cells expressing sh-scramble or SQLE shRNA was determined by wound-healing assay. Scale bar: 200 μm. (**I**) Migration capacity of H226 cells expressing vector or SQLE overexpression was determined by wound-healing assay. Scale bar: 200 μm. $^{**}P < 0.01$; $^{***}P < 0.001$; $^{****}P < 0.0001$.

To test whether TBF can inhibit LUSC growth *in vivo*, we selected DBA2J mice, which were the most suitable for inoculation with LUSC mouse tumor cell line KLN205 [20, 21]. TBF has shown encouraging efficacy in an assortment of tumor types in previous investigations [8, 22, 23], however, it is unclear whether TBF is therapeutically beneficial in LUSC. Six-week-old DBA2J mice were inoculated in the right flank with 3×10^6 KLN-205 cells. Six days following inoculation, TBF was administered intraperitoneally at a dose of 80 mg/kg q2d, with PBS serving as the control (Veh) treatment. After receiving six consecutive treatments over a period of 12 days, the mice were sacrificed on the 18th day following inoculation with KLN205 cells (Fig. 4G). Compared with those treated with Veh, LUSC primary tumors subcutaneously inoculated with TBF shrank significantly (Fig. 4H). The mean weight of the tumor mass was also significantly different between the two group (Fig. 4I). Similarly, tumor size was decreased markedly in TBF-treated mice compared with those treated with Veh (Fig. 4J). However, the body weight of DBA2J mice was not impacted noticeably before and after treatment (Fig. 4K). IHC analysis showed that the expression of Ki67 was lower in the TBF treatment group than in the Veh group, nevertheless, there was no noticeable change in the expression of SQLE (Fig. 4L). As a result, we verified that the SQLEi TBF hampered the proliferation and development of tumors *in vivo* and *in vitro*.

Suppression of SQLE directly induces apoptosis and augments the accumulation of mitochondrial ROS

To comprehend the mechanism by which SQLE deficiency causes inhibition of tumor proliferation, we analyzed the NES of different regulated cell death pathways such as apoptosis, pyroptosis, ferroptosis and necrosis from RNA-seq data of SQLE-KD cells. The apoptotic pathway was the most primary signaling ingene enrichment among these cell death pathways in the sh-SQLE group (Fig. 5A). GSEA and heatmap revealed that

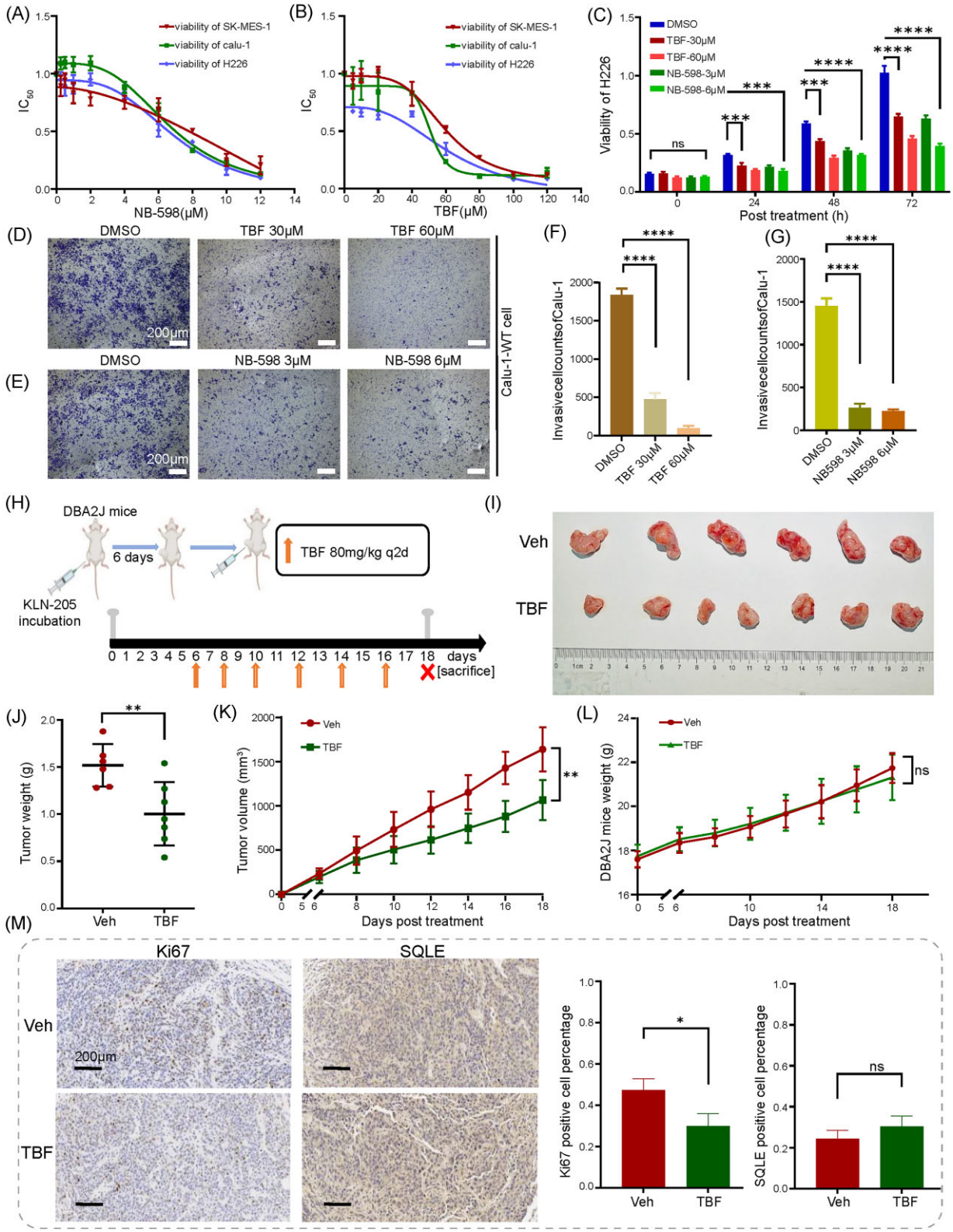

Figure 4. SQLE inhibitors suppress LUSC cells *in vitro* and *in vivo*. Viability of SK-MES-1, Calu-1 and H226 cells treated with different concentrations of TBF (**A**) or NB-598 (**B**). (**C**) Growth ratios of SK-MES-1, Calu-1 and H226 at 24, 48 and 72 h after adding TBF or NB-598, by CCK-8 assay. (**D**–**G**) Crystal violet staining for cell invasion experiment and statistical plot of Calu-1 cells after the addition of TBF (D) or NB-598 (E) via transwell chambers. Statistical analysis of treatment with (F) TBF or (G) NB-598. Scale bar: 200 μm. (**H**) Pattern diagram of DBA2J mice inoculated with LUSC mouse KLN-205 cells and the time points of administration of treatments with vehicle (PBS) ($n = 6$) or TBF (80 mg/kg, administered intraperitoneally, q2d, $n = 7$). (**I**) Subcutaneous tumor mass after administration of treatment with vehicle (Veh) and TBF six times. (**J**–**L**) Changes over time in tumor weight (J), tumor volume (K) and DBA2J mice weight (L) in vehicle or TBF-treated groups. (**M**) Representative images of immunohistochemistry for Ki67 (left) and SQLE (right) staining in xenografts derived from KLN-205 cells. Scale bar: 100 μm. $^{*}P < 0.05$; $^{**}P < 0.01$; $^{***}P < 0.001$; $^{****}P < 0.0001$; ns not significant.

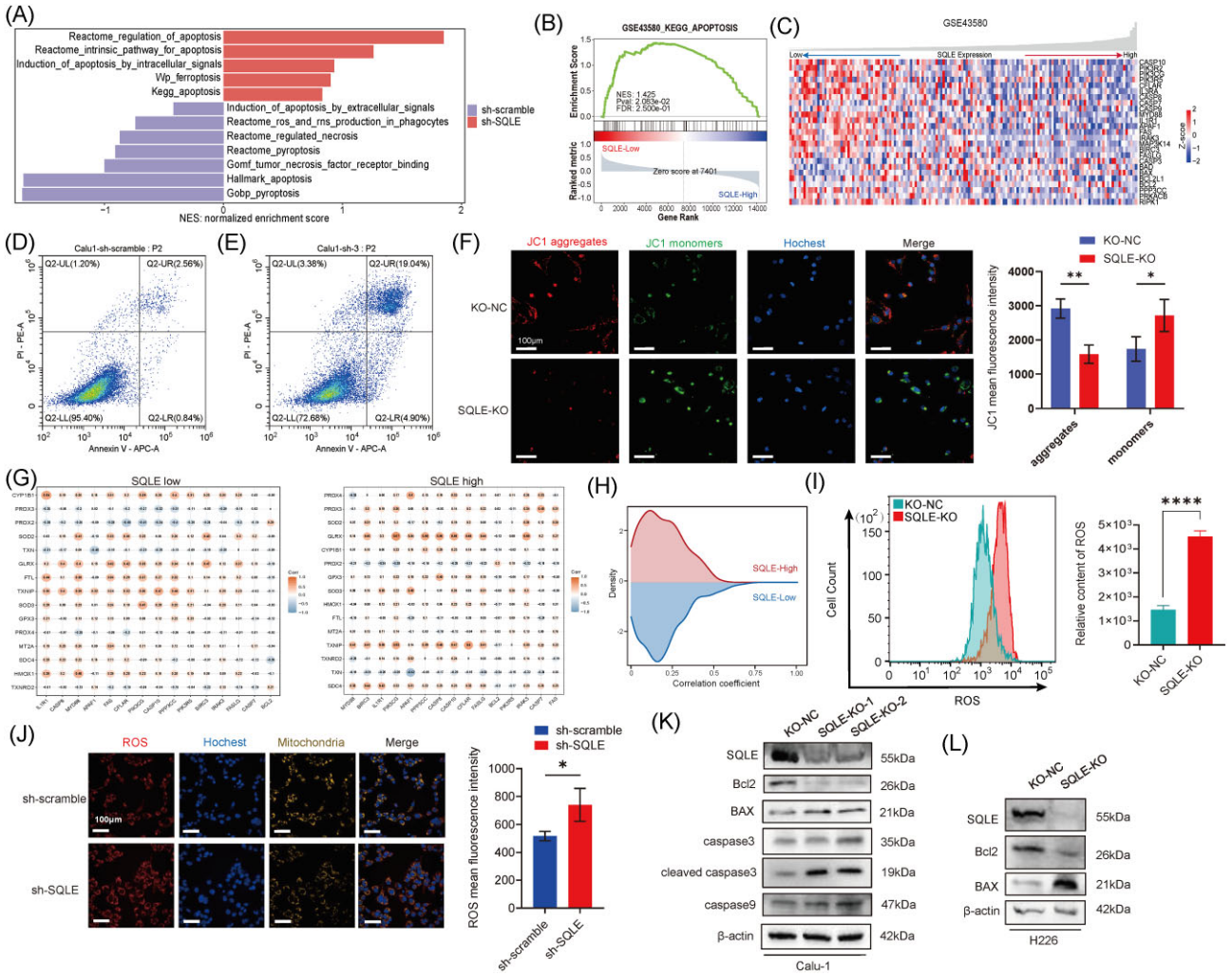

Figure 5. Repression of SQLE induces apoptosis and enhances the accumulation of mitochondrial ROS. (**A**) Enrichment of cell death pathways by GSEA in sh-scramble vs sh-SQLE of SK-MES-1. (**B**) GSEA plot of the apoptosis signaling pathway in SQLE low- or high-expression groups of the GSE43580 dataset. (**C**) Heatmap revealing relative gene expression of apoptosis in SQLE low- or high-expression groups of the GSE43580 dataset. Representative results of annexin V/propidium iodide staining of Calu-1 cells expressing sh-scramble (**D**) or SQLE shRNA (**E**). (**F**) Representative images and statistical analysis of mitochondrial membrane potential high-content screening system of a confocal microscope (HCSSCM) using the JC-1 test (green fluorescence represents monomers; red fluorescence represents aggregates). Scale bar: 100 μm. (**G**) Pearson's correlation analysis was estimated among the core genes of ROS (*y*-axis) and apoptosis (*x*-axis) in the SQLE-low expression group (left) and SQLE-high expression group (right) of the GSE43580 dataset. The size of the circles and the darkness of color are proportionate to the correlation coefficient. Red and blue represent positive and negative correlations, respectively. (**H**) Curves represent the distribution of correlation coefficients in SQLE-low or -high expression groups of the GSE43580 dataset. (**I**) Flow cytometry histogram showing the counts and statistical analysis of ROS in Calu-1 with or without SQLE knockout cells. (**J**) Representative images and statistical analysis of HCSSCM with detection of ROS (deep red) and mitochondria (orange red). Scale bar: 100 μm. Western blotting analysis showing the expression level of SQLE, BAX, Bcl2, caspase 3, cleaved caspase 3 and caspase 9 in Calu-1 (**K**) and H226 (**L**) cells with or without SQLE knockout. $^*P < 0.05$; $^{**}P < 0.01$; $^{****}P < 0.0001$.

the apoptosis pathway was also enriched in SQLE-low expression patients (SQLE-low) in the GSE43580 or TCGA-LUSC datasets (Fig. 5B, C and supplementary Fig. S3A, B, see online supplementary material). To further determine whether deletion of SQLE promotes apoptosis, we verified it using KD or knockout (KO) of SQLE from multiple perspectives. Initially, we found SQLE-KD significantly induced apoptosis (quadrant Q2-UR 19.04%) compared to control (Q2-UR 2.56%) using propidium iodide (PI) and annexin V (Fig. 5D, E). Furthermore, we constructed a SQLE-KO cell line employing the CRISPR-Cas9 system and further analyzed mitochondrial membrane potential by the JC-1 assay. The red and green fluorescence intensity represent JC-1 aggregates and monomers, respectively. The augmentation of monomers and an increase in the green/red ratio meant mitochondrial membrane depolarization and apoptosis. Compared with control, SQLE-KO displayed fewer aggregates and more monomers using the high-content screening system of a confocal microscope (HCSSCM), which indicated an increase in apoptosis (Fig. 5F).

Apoptosis is typically accompanied by a massive amount of ROS production [13]. Subsequently, we investigated whether reduced SQLE expression was linked to the generation of ROS and activation of the apoptotic pathway. A correlation heatmap was employed to ascertain the differences in correlation between ROS/antioxidant genes and apoptotic gene expression in the SQLE high/low group. The results indicated higher correlation between ROS/antioxidant genes and apoptosis genes in the SQLE-low group in comparison with the SQLE-high group,

both in the GSE43580 and TCGA-LUSC datasets (Fig. 5G, H and Supplementary Fig. S3C, D). Correspondingly, ROS levels were elevated in SQLE-KO and TBF-treated LUSC cells as measured by flow cytometry (Fig. 5I, Supplementary Fig. S4A). Moreover, aberrant mitochondrial function-induced ROS could bring about endogenous apoptosis [24, 25]. To evaluate whether the SQLE-KO-triggered ROS originated from mitochondria, the fluorescence positions of ROS (labelled deep red) and mitochondria (labelled orange red) were found to overlap using the HCSSCM (Fig. 5J). Apoptosis is mostly carried out by the caspase family, which includes caspase-3, cleaved caspase-3 (the primary apoptotic executor) and caspase-9 (apoptotic cascade amplification) [26, 27]. It was also discovered that cleaved caspase-3 and caspase-9, but not caspase-3, were upregulated in SQLE-KD or TBF-treated cells (Fig. 5K, supplementary Fig. S4B, see online supplementary material). In addition, Bcl2 was downregulated and Bax was upregulated in SQLE-KO cells compared to control in both Calu-1 and H226 cells (Fig. 5K, L). Hence, we certified that SQLE intervention induced apoptosis mainly through the accumulation of mitochondrial ROS.

Knockout of SQLE suppresses lipid peroxidation and effectively eliminates LUSC by synergizing with GPX4 inhibitor RSL3

Previous studies suggest that tumor cells can respond to increased ROS levels by expressing high levels of antioxidant proteins [10, 28]. In addition, ferroptosis is essentially an Fe(II)-dependent lipid peroxidation carried out by an overabundance of ROS [14, 15]. We also observed the potential involvement of SQLE-KD in ferroptosis (Fig. 5A). To further determine whether SQLE simultaneously regulates ferroptosis, the level of lipid peroxidation (C11-BODIPY probe) was examined in SQLE-KO cells using HCSSCM fluorescence. However, SQLE-KO cells had lower levels of oxidized lipids (green) compared to control cells, and the difference in non-oxidized fractions (orange-red) was not statistically significant (Fig. 6A, B). SQLE deletion could repress lipid peroxidation rather than increase ROS. It was consistently found that the ferroptosis pathway (including ferroptosis inducer and ferroptosis suppressor genes) was significantly strengthened in SQLE-low samples from the GSE4573 and TCGA datasets (Fig. 6C and supplementary Fig. S5A, see online supplementary material).

Ferroptosis resistance factors, such as GPX4 and xCT [Cystine/glutamic acid reverse transporter (System X(c) (-)), also known as solute carrier family 7 member 11 (SLC7A11)], can be amplified and overexpressed to mitigate ferroptosis [29–31]. In both H226 and Calu-1 SQLE-KO cell lines, GPX4 and xCT protein expression was upregulated (Fig. 6D). In a similar vein, TBF treatment also heightened the protein expression of GPX4 and xCT (supplementary Fig. S5B). Moreover, SQLE-KO or the addition of TBF and NB-598 resulted in the accumulation of squalene, a powerful reducing metabolite and the upstream substrate of SQLE (Fig. 6E, supplementary Fig. S5C), which has been shown to suppress peroxidation [16]. In addition, we conducted HCSSCM fluorescence analysis and found that SQLE-KO led to lower intracellular Fe(II) levels (Fig. 6F). This demonstrated that SQLE-KO mediates resistance to ferroptosis. In summary, although SQLE deficiency induces apoptosis and ROS, lipid peroxidation was restrained by the reactivation of corresponding protein expression that is resistant to ferroptosis, thereby maintaining cell survival. To better understand if ferroptosis inducers can completely eliminate SQLE-KO cells, we treated them with the GPX4 blocker RSL3. We observed the proliferation status of SQLE-KO cells every 12 h after treatment with RSL3 at 0.5 μM [32]. The results showed a significant reduction in cell proliferation compared to the control cells and the vehicle (treatment with DMSO) (Fig. 6G). After treating SQLE-KO and KO-NC with 0.5 μM RSL3 for 24 h, we observed a significant impairment in cell migration in SQLE-KO (Fig. 6H). These results suggest that the combined blockade of SQLE and GPX4 could effectively inhibit the proliferation and migration of LUSC cells.

Furthermore, KLN-205 mice tumor cells were inoculated subcutaneously in the right flank of 6-week-old DBA2J mice. Mice were initially inoculated with 200×10^6 cells. According to previous research, the dose of RSL3 administered to mice was 50 mg/kg individually [33]. Hence, after inoculating KLN-205 in subcutaneous tumor-bearing mice for 6 days, with PBS as control (vehicle), RSL3 was given by intraperitoneal administration at a dose of 50 mg/kg alone or in combination with TBF at a dose of 80 mg/kg q2d. Ultimately, after five consecutive rounds of combined therapy, mice were sacrificed and the weight and size of the subcutaneous tumors were analyzed. Generally, TBF in concert with RSL3 dramatically shrank the average size and weight of LUSC mice tumors compared with a vehicle and monotherapy group (Fig. 6I–K).

Discussion

Cholesterol synthesis plays a crucial role in tumor development. SQLE, a key rate-limiting enzyme in the synthesis of oxysterols, is involved in the development of several tumors through multiple mechanisms. However, SQLE has shown paradoxical phenotypes with opposite results in different studies. While most studies suggest that it is a carcinogenic factor, some studies have reported contradictory findings. For instance, SQLE promotes the activation of the PI3K-AKT-mTOR pathway through ROS-dependent DNA methylation in the development of non-alcoholic fatty liver disease (NAFLD)-induced hepatocellular carcinoma. It may be a crucial target for treating hepatocellular carcinoma [8]. Additionally, it has been proposed that the molecular mechanism driving SQLE expression may involve p53 deletion or mutation [23]. SQLE also contributes to cholesterol-dependent lipid raft formation and promotes the activation of the Src-PI3K-Akt signaling pathway in pancreatic cancer [7]. In addition, SQLE plays a cancer-promoting role among other cancer types [19, 34, 35]. Conversely, low expression of SQLE was involved in colorectal cancer metastasis [9]. In our study, SQLE was highly expressed in LUSC patients, and high levels of SQLE directly correlated with poor prognosis for such patients. Inconsistently, SQLE contributed to the proliferative, migratory and invasive capacity of a LUSC cell line. Depletion of SQLE tended to induce cell death and depression of cell viability.

TBF and NB-598, which are widely accessible SQLEi, have been shown to impede the growth and proliferation of HCC, pancreatic cancer and prostate cancer in both *in vitro* and *in vivo* studies [7, 8, 23, 35, 36]. Our research also confirmed the suppressive effect of TBF and NB-598 on LUSC proliferation and invasion. Although TBF treatment was able to reduce tumor size and weight to some extent in a subcutaneously grafted tumor model, the mice still had a significant tumor burden. In addition, although high concentrations of TBF could inhibit SQLE expression in LUSC cells, lower concentrations of SQLEi may boost protein expression of SQLE, consistent with a previous investigation [19]. We hypothesized that the tumor-killing effect of SQLEi was probably not directly through inhibition of SQLE expression. It is important to note that SQLEi has some toxicity. For instance, TBF exhibits hepatotoxicity to a certain degree, while NB-598 has dose-limiting gastrointesti-

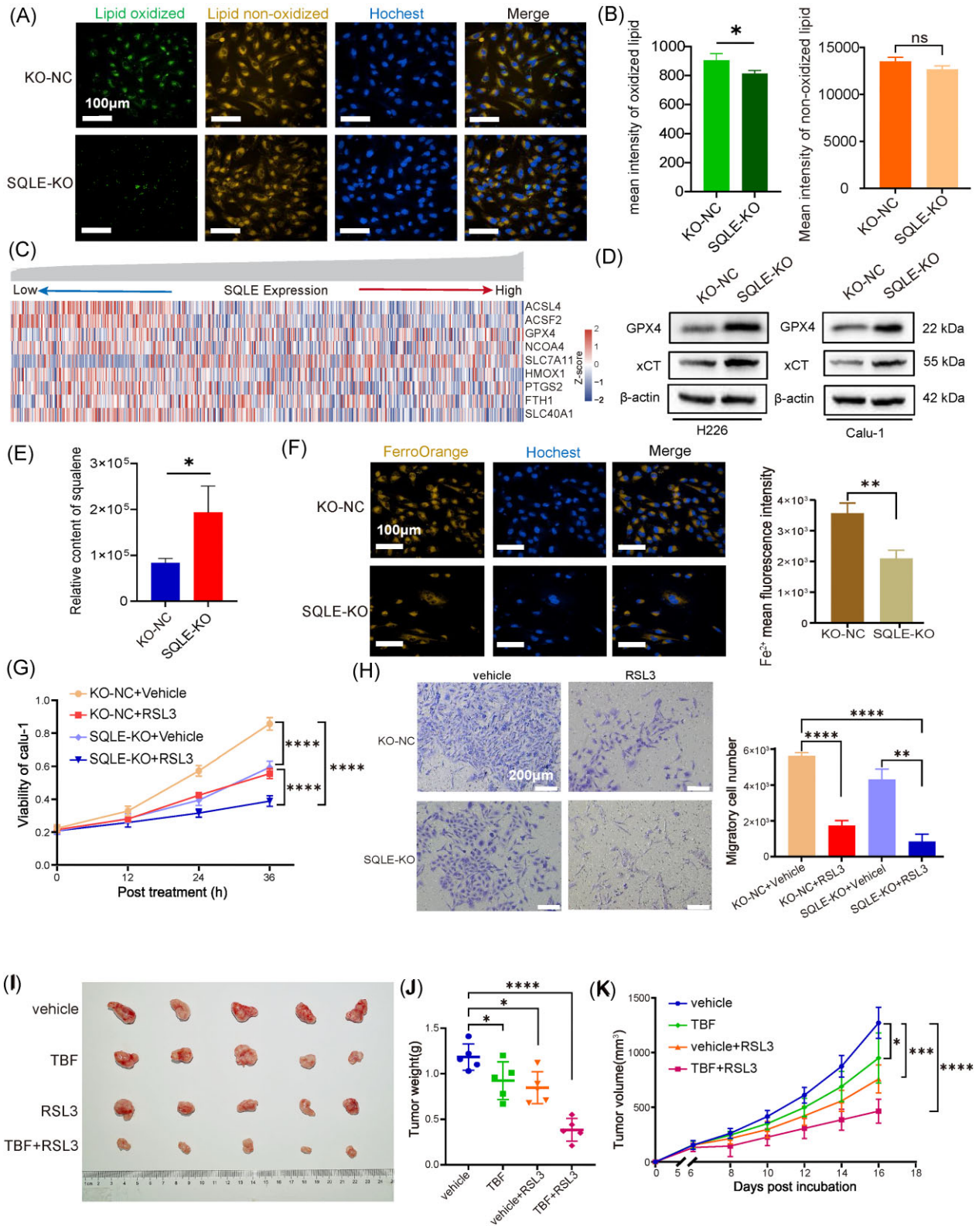

Figure 6. Prevention of SQLE in combination with ferroptosis inducer (RSL3) can accelerate LUSC cell death. Representative image (**A**) and statistical analysis (**B**) of HCSSCM with detection of oxidized lipid (green) and non-oxidized lipid (orange red) in SQLE knockout cells. Scale bar: 100 μm. (**C**) GSEA plot and heatmap showing relative gene expression of the antioxidant pathway in SQLE low- or high-expression groups of the TCGA dataset. (**D**) Western blot analysis showing the expression level of GPX4 and xCT in SQLE-KO Calu-1 and H226 cells, respectively. (**E**) Statistical analysis showing the relative content of squalene in Calu-1 cells with or without SQLE knockout. (**F**) Representative image and statistical analysis of HCSSCM with detection of Fe(II) by FerroOrange (orange red). Scale bar: 100 μm. (**G**) Growth curves of SQLE knockout and control Calu-1 cells with vehicle and RSL3 detected by CCK-8. (**H**) Crystal violet staining and statistical analysis for cell migration experiment of SQLE knockout (bottom) and control (top) Calu-1 cells with vehicle and RSL3 (0.5 μM for 24 h). Scale bar: 200 μm. (**I**) Images of isolated tumors from a tumor model grafted subcutaneously with KLN205 cells treated with vehicle (PBS), TBF (80 mg/kg, intraperitoneal, q2d), RSL3 (50 mg/kg, intraperitoneal, q2d) and TBF (80 mg/kg, intraperitoneal, q2d) plus RSL3 (50 mg/kg, intraperitoneal, q2d) ($n = 5$ per group), respectively. Continuous time points of isolated tumor weight (**J**) and tumor volume (**K**) in tumors treated with vehicle, TBF, RSL3 and TBF plus RSL3, respectively. *$P < 0.05$; **$P < 0.01$; ***$P < 0.001$; ****$P < 0.0001$.

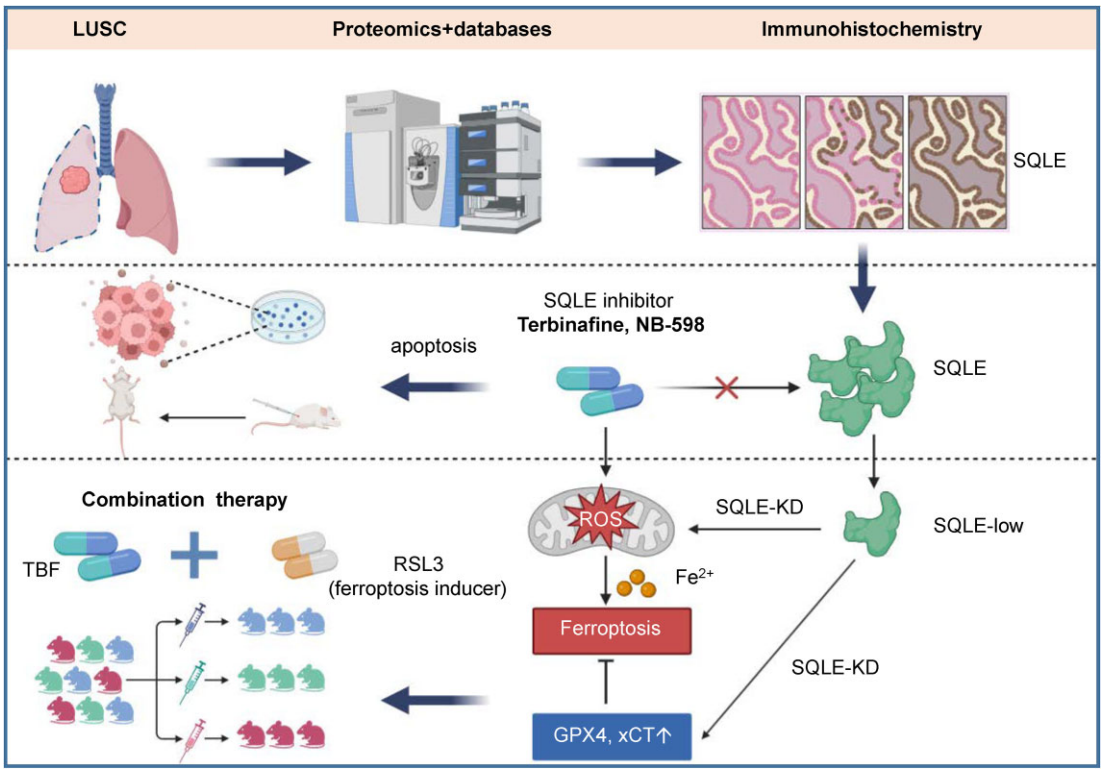

Figure 7. A model of screening SQLE in LUSC, its mechanism of signal transduction and a treatment strategy. We used proteomics and databases to screen for SQLE, a key metabolic target of cholesterol in LUSC. Intervention with SQLE or its inhibitors can suppress tumor proliferation *in vivo* and *in vitro* mainly through the augmentation of ROS and apoptosis. In addition, SQLE deletion can counteract oxidative stress and lipid peroxidation through inducing the upregulation of GPX4 and xCT. Combined intervention with SQLE and a ferroptosis inducer can achieve better therapeutic outcomes for LUSC. The drawing was created with biorender.com.

nal toxicity [37, 38]. Our experiments indicate that the significant toxic effects of TBF may primarily induce ROS-mediated tumor cell death. Similarly, we observed ROS accumulation in the SQLE-KO cell line of LUSC. Repeated *in vitro* tests demonstrated that exposing LUSC cells to >80 μM TBF for 48 h generally inhibited >80% of cell growth. Therefore, the mechanism by which SQLEi TBF suppresses tumor growth *in vivo* and *in vitro* is mainly by increasing ROS, rather than directly suppressing the expression of SQLE protein

We found that SQLE-KD cells are predominantly enriched in the apoptotic pathway, which is associated with regulated cell death. At the cellular level, we observed that the deficiency of SQLE activated endogenous apoptosis, which is dependent on caspase family proteins (especially cleaved caspase 3), Bax and Bcl2, an increase of annexin V and PI as well as mitochondrial membrane potential depolarization. Additionally, apoptotic genes are mainly expressed in SQLE-low samples in the GEO or TCGA datasets. In these clinical samples, the SQLE-low group is more strongly associated with apoptosis and ROS/antioxidant than the SQLE-high group, which means activation of the antioxidant system. It is important to note that ROS has a dual role. Sustained ROS can cause DNA damage and genetic instability, leading to oxidative stress-induced tumor cell death [11]. However, an appropriate degree of ROS might activate pro-tumor signaling, promoting cell survival and proliferation. Tumor cells often express high levels of antioxidant proteins to counteract elevated levels of ROS, which can establish redox homeostasis while maintaining pro-tumor signaling and resistance to apoptosis [10]. Our study determined that GPX4 and xCT were significantly activated in SQLE-KO or TBF treated cells, which prevented LUSC cells from undergoing lipid peroxidation and ferroptosis. Additionally, Anaplastic Lymphoma Kinase positive (ALK+) lymphoma cells with low expression of SQLE promote tumor progression through resisting ferroptosis [39]. The SQLE upstream substrate, squalene, is a reductive metabolite that can protect cancer cells from oxidative stress [39]. Our data also illustrate that SQLEi or SQLE-KO induced an accumulation of squalene by targeting metabolomics, thus protecting cancer cells from lipid peroxidation and oxidative stress. In conclusion, SQLE-KO represents ferroptosis resistance to counteract more production of ROS.

Generally speaking, SQLE may play a unique role in LUSC. It can be involved in pro-carcinogenesis, and SQLE deficiency significantly triggers mitochondria-dependent ROS accumulation and apoptosis of LUSC. Interestingly, intervening with SQLE can also lead to ROS/antioxidant gene enrichment and weaken lipid peroxidation simultaneously. Our data revealed that SQLE-KO induced an increase in ferroptosis resistance factors such as GPX4, representing attenuated lipid peroxidation. However, GPX4 expression was associated with recurrence and metastasis of tumors such as breast and gastric cancers [40, 41]. Tumors in mice subcutaneously treated with a combination of SQLEi inhibitors still had a large tumor load. Therefore, a ferroptosis inducer RSL3, manifested a remarkable therapeutic effect , combined with depletion SQLE in LUSC.

However, there are still some unanswered questions. For instance, it is unclear whether SQLE affects the entry of NRF2 into the nucleus to initiate antioxidant gene activation, and how SQLE functions specifically in chromatin or cytoplasm. Additionally, it

is uncertain whether SQLEi intervenes in the transcription of the antioxidant system through nuclear entry. Further investigation in this regard is necessary.

In summary, high expression of SQLE can directly promote tumor development. Deletion of SQLE or TBF treatment augments ROS accumulation and apoptosis. However, anti-oxidative stress plays a compensatory role by modulating upregulation of GPX4 in response to lipid peroxidation, thus sustaining tumor survival. When we incorporated the ferroptosis inducer RSL3 into the regimen, the tumor was significantly eliminated. This suggests that a combination therapy targeting SQLE and a ferroptosis inducer may achieve better therapeutic effects.

Conclusion

In conclusion, our study demonstrates that SQLE plays a significant role in the development of LUSC. Targeted SQLE inhibition can effectively reduce cell proliferation and tumor growth by inducing ROS accumulation and apoptosis. Furthermore, the compensatory antioxidant pathway, such as GPX4 upregulation, counterbalances ROS accumulation and impairs lipid peroxidation to promote tumor cell survival. The GPX4 suppressor RSL3, in synergy with inhibition of SQLE, could significantly suppress LUSC growth *in vitro* and *in vivo* (Fig. 7).

Acknowledgments

We thank the Proteomics Platform of West China Hospital of Sichuan University for targeted metabolomics and the confocal microscope. This work was supported by the National Natural Science Foundation of China (Grant No. 92159302, W.L.); Science and Technology Project of Sichuan (Grant No. 2022ZDZX0018, W.L.); 1.3.5 project for disciplines of excellence, West China Hospital, Sichuan University (Grant No. ZYGD22009, W.L.). This work was also supported by National Key R&D program of China (Grant No. 2022YFC2505000), NSFC general program (Grant No. 82272796), NSFC special program (Grant No. 82241229), CAMS Innovation Fund for Medical Sciences (Grant No. CIFMS 2022-I2M-1–009), CAMS Key Laboratory of Translational Research on Lung Cancer (Grant No. 2018PT31035), and the Aiyou foundation (Grant No. KY201701).

Author contributions

Conceptualization: G.L., W.L. and J.W.; administrative support: J.W., W.L. and L.Z.; data analysis and curation: G.L. and L.C.; investigation and validation: L.Z. and H.B.; writing—original draft: G.L. and J.W.; funding acquisition: J.W. and W.L. All authors have read and agreed to the published version of the manuscript.

Supplementary data

Supplementary data are available at *PCMEDI* online.

Conflict of interest

None declared. As a co-Editor-in-Chief of *Precision Clinical Medicine*, the corresponding author W.L. was blinded from reviewing and making decision on this manuscript.

Ethics

This project was approved by the Ethics Committee of the Cancer Hospital of the Chinese Academy of Medical Sciences and West China Hospital of Sichuan University (Ethical code 20 221 230 001 and 2022/12/29 of approval). The animal experiment protocol was approved by the Animal Care and Use Committee of West China Hospital of Sichuan University and conform to the guidelines on the protection of animals used for scientific purposes.

Reference

1. Satpathy S, Krug K, Jean Beltran PM *et al.* A proteogenomic portrait of lung squamous cell carcinoma. *Cell* 2021;**184**:4348–4371 e40. https://doi.org/10.1016/j.cell.2021.07.016.
2. Paik PK, Pillai RN, Lathan CS *et al.* New treatment options in advanced squamous cell lung cancer. *Am Soc Clin Oncol Educ Book* 2019;**39**:e198–206. https://doi.org/10.1200/EDBK_237829.
3. Heist RS, Sequist LV, Engelman JA. Genetic changes in squamous cell lung cancer: a review. *J Thorac Oncol* 2012;**7**:924–33. https://doi.org/10.1097/JTO.0b013e31824cc334.
4. Lau SCM, Pan Y, Velcheti V *et al.* Squamous cell lung cancer: current landscape and future therapeutic options. *Cancer Cell* 2022;**40**:1279–93. https://doi.org/10.1016/j.ccell.2022.09.018.
5. Goodwin J, Neugent ML, Lee SY *et al.* The distinct metabolic phenotype of lung squamous cell carcinoma defines selective vulnerability to glycolytic inhibition. *Nat Commun* 2017;**8**:15503. https://doi.org/10.1038/ncomms15503.
6. Guo C, Wan R, He Y *et al.* Therapeutic targeting of the mevalonate-geranylgeranyl diphosphate pathway with statins overcomes chemotherapy resistance in small cell lung cancer. *Nat Cancer* 2022;**3**:614–28. https://doi.org/10.1038/s43018-022-00358-1.
7. Xu R, Song J, Ruze R *et al.* SQLE promotes pancreatic cancer growth by attenuating ER stress and activating lipid rafts-regulated src/PI3K/Akt signaling pathway. *Cell Death Dis* 2023;**14**:497. https://doi.org/10.1038/s41419-023-05987-7.
8. Liu D, Wong CC, Fu L *et al.* Squalene epoxidase drives NAFLD-induced hepatocellular carcinoma and is a pharmaceutical target. *Sci Transl Med* 2018 Apr 18;**10**(437): eaap9840. https://doi.org/10.1126/scitranslmed.aap9840.
9. Jun SY, Brown AJ, Chua NK *et al.* Reduction of squalene epoxidase by cholesterol accumulation accelerates colorectal cancer progression and metastasis. *Gastroenterology* 2021;**160**:1194–1207 e28. https://doi.org/10.1053/j.gastro.2020.09.009.
10. Sabharwal SS, Schumacker PT. Mitochondrial ROS in cancer: initiators, amplifiers or an Achilles' heel? *Nat Rev Cancer* 2014;**14**:709–21. https://doi.org/10.1038/nrc3803.
11. Scott TL, Rangaswamy S, Wicker CA *et al.* Repair of oxidative DNA damage and cancer: recent progress in DNA base excision repair. *Antioxid Redox Signal* 2014;**20**:708–26. https://doi.org/10.1089/ars.2013.5529.
12. Rojo De La Vega M, Chapman E, Zhang DD. NRF2 and the hallmarks of cancer. *Cancer Cell* 2018;**34**:21–43. https://doi.org/10.1016/j.ccell.2018.03.022.
13. Hayes JD, Dinkova-Kostova AT, Tew KD. Oxidative stress in cancer. *Cancer Cell* 2020;**38**:167–97. https://doi.org/10.1016/j.ccell.2020.06.001.
14. Von Krusenstiern AN, Robson RN, Qian N *et al.* Identification of essential sites of lipid peroxidation in ferroptosis. *Nat Chem Biol* 2023;**19**:719–30. https://doi.org/10.1038/s41589-022-01249-3.

15. Su L-J, Zhang J-H, Gomez H *et al.* Reactive oxygen species-induced lipid peroxidation in apoptosis, autophagy, and ferroptosis. *Oxid Med Cell Longev* 2019;**2019**:5080843. https://doi.org/10.1155/2019/5080843.
16. Micera M, Botto A, Geddo F *et al.* Squalene: more than a step toward sterols. *Antioxidants (Basel)* 2020;**9** (8):688. https://doi.org/10.3390/antiox9080688.
17. Mahoney CE, Pirman D, Chubukov V *et al.* A chemical biology screen identifies a vulnerability of neuroendocrine cancer cells to SQLE inhibition. *Nat Commun* 2019;**10**:96. https://doi.org/10.1038/s41467-018-07959-4.
18. Padyana AK, Gross S, Jin L *et al.* Structure and inhibition mechanism of the catalytic domain of human squalene epoxidase. *Nat Commun* 2019;**10**:97. https://doi.org/10.1038/s41467-018-07928-x.
19. Hong Z, Liu T, Wan L *et al.* Targeting squalene epoxidase interrupts homologous recombination via the ER stress response and promotes radiotherapy efficacy. *Cancer Res* 2022;**82**:1298–312. https://doi.org/10.1158/0008-5472.CAN-21-2229.
20. O-Sullivan I, Chopra A, Kim TS *et al.* New strategy for the identification of squamous carcinoma antigens that induce therapeutic immune responses in tumor-bearing mice. *Cancer Gene Ther* 2007;**14**:389–98. https://doi.org/10.1038/sj.cgt.7701023.
21. Kaneko T, LePage GA. Growth characteristics and drug responses of a murine lung carcinoma in vitro and in vivo. *Cancer Res* 1978;**38**:2084–90.
22. Hu L-P, Huang W, Wang X *et al.* Terbinafine prevents colorectal cancer growth by inducing dNTP starvation and reducing immune suppression. *Mol Ther* 2022;**30**:3284–99. https://doi.org/10.1016/j.ymthe.2022.06.015.
23. Sun H, Li L, Li W *et al.* p53 transcriptionally regulates SQLE to repress cholesterol synthesis and tumor growth. *EMBO Rep* 2021;**22**:e52537. https://doi.org/10.15252/embr.202152537.
24. Zhang B, Pan C, Feng C *et al.* Role of mitochondrial reactive oxygen species in homeostasis regulation. *Redox Rep* 2022;**27**:45–52. https://doi.org/10.1080/13510002.2022.2046423.
25. Li N, Ragheb K, Lawler G *et al.* Mitochondrial complex I inhibitor rotenone induces apoptosis through enhancing mitochondrial reactive oxygen species production. *J Biol Chem* 2003;**278**:8516–25. https://doi.org/10.1074/jbc.M210432200.
26. Araya LE, Soni IV, Hardy JA *et al.* Deorphanizing caspase-3 and caspase-9 substrates In and out of apoptosis with deep substrate profiling. *ACS Chem Biol* 2021;**16**:2280–96. https://doi.org/10.1021/acschembio.1c00456.
27. Nicholson DW, Ali A, Thornberry NA *et al.* Identification and inhibition of the ICE/CED-3 protease necessary for mammalian apoptosis. *Nature* 1995;**376**:37–43. https://doi.org/10.1038/376037a0.
28. Kudo Y, Sugimoto M, Arias E *et al.* PKClambda/iota loss induces autophagy, oxidative phosphorylation, and NRF2 to promote liver cancer progression. *Cancer Cell* 2020;**38**:247–262 e11. https://doi.org/10.1016/j.ccell.2020.05.018.
29. Yan Y, Teng H, Hang Q *et al.* SLC7A11 expression level dictates differential responses to oxidative stress in cancer cells. *Nat Commun* 2023;**14**:3673. https://doi.org/10.1038/s41467-023-39401-9.
30. Ouyang S, Li H, Lou L *et al.* Inhibition of STAT3-ferroptosis negative regulatory axis suppresses tumor growth and alleviates chemoresistance in gastric cancer. *Redox Biol* 2022;**52**:102317. https://doi.org/10.1016/j.redox.2022.102317.
31. Yang WS, Sriramaratnam R, Welsch ME *et al.* Regulation of ferroptotic cancer cell death by GPX4. *Cell* 2014;**156**:317–31. https://doi.org/10.1016/j.cell.2013.12.010.
32. Wohlhieter CA, Richards AL, Uddin F *et al.* Concurrent mutations in STK11 and KEAP1 promote ferroptosis protection and SCD1 dependence in lung cancer. *Cell Rep* 2020;**33**:108444. https://doi.org/10.1016/j.celrep.2020.108444.
33. Jia M, Qin D, Zhao C *et al.* Redox homeostasis maintained by GPX4 facilitates STING activation. *Nat Immunol* 2020;**21**:727–35. https://doi.org/10.1038/s41590-020-0699-0.
34. Shangguan X, Ma Z, Yu M *et al.* Squalene epoxidase metabolic dependency is a targetable vulnerability in castration-resistant prostate cancer. *Cancer Res* 2022;**82**:3032–44. https://doi.org/10.1158/0008-5472.CAN-21-3822.
35. Kalogirou C, Linxweiler J, Schmucker P *et al.* MiR-205-driven downregulation of cholesterol biosynthesis through SQLE-inhibition identifies therapeutic vulnerability in aggressive prostate cancer. *Nat Commun* 2021;**12**:5066. https://doi.org/10.1038/s41467-021-25325-9.
36. Zhao F, Huang Y, Zhang Y *et al.* SQLE inhibition suppresses the development of pancreatic ductal adenocarcinoma and enhances its sensitivity to chemotherapeutic agents in vitro. *Mol Biol Rep* 2022;**49**:6613–21. https://doi.org/10.1007/s11033-022-07504-z.
37. Nagaraja R, Olaharski A, Narayanaswamy R *et al.* Preclinical toxicology profile of squalene epoxidase inhibitors. *Toxicol Appl Pharmacol* 2020;**401**:115103. https://doi.org/10.1016/j.taap.2020.115103.
38. Meletiadis J, Chanock S, Walsh TJ. Defining targets for investigating the pharmacogenomics of adverse drug reactions to antifungal agents. *Pharmacogenomics* 2008;**9**:561–84. https://doi.org/10.2217/14622416.9.5.561.
39. Garcia-Bermudez J, Baudrier L, Bayraktar EC *et al.* Squalene accumulation in cholesterol auxotrophic lymphomas prevents oxidative cell death. *Nature* 2019;**567**:118–22. https://doi.org/10.1038/s41586-019-0945-5.
40. Wang Y, Zheng L, Shang W *et al.* Wnt/beta-catenin signaling confers ferroptosis resistance by targeting GPX4 in gastric cancer. *Cell Death Differ* 2022;**29**:2190–202. https://doi.org/10.1038/s41418-022-01008-w.
41. Liu W, Chakraborty B, Safi R *et al.* Dysregulated cholesterol homeostasis results in resistance to ferroptosis increasing tumorigenicity and metastasis in cancer. *Nat Commun* 2021;**12**:5103. https://doi.org/10.1038/s41467-021-25354-4.

Received 12 March 2024; accepted 29 April 2024. published 8 May 2024